CAAP Quarterly Report

Date of Report: April 10th 2020

Prepared for: *U.S. DOT Pipeline and Hazardous Materials Safety Administration*

Contract Number: 693JK31850008CAAP

Project Title: Fluorescent Chemical Sensor Array for Detecting and Locating Pipeline Internal Corrosive Environment

Prepared by: Dr. Ying Huang, Dr. Wenfang Sun, and Dr. Hao Wang

Contact Information: Dr. Ying Huang, Email: ying.huang@ndsu.edu, Phone: 701.231.7651

For quarterly period ending: April 10th 2020

Business and Activity Section

(a) Contract Activity

Discussion about contract modifications or proposed modifications:

Proposed modification: *We would like to request a three-month "No Cost Extension" to end the project on December 31 2021 instead of completing the project in September 31 2021. There is no request for additional budget, only request the extension of the project duration for three more months so that we can make up the time we will lose during this corona outbreak for research. Your consideration of this request is highly appreciated by NDSU researchers and graduate students.*

Discussion about materials purchased:

None.

(b) Status Update of Past Quarter Activities

Task 2.1, 2.2, 2.3, Task 3

(c) Cost share activity

Tuition Waiver for two graduate students with $9,364 of cost share in this quarter.

(d) Task 2: Development of Fluorescent/Colorimetric Chemical Sensor Array for Internal Corrosive Water Detection

We continue working on the four subtasks during this quarter including Task 2.1 (Development of Fluorescent/Colorimetric Chemical Sensor Array), Task 2.2 (Calibration of the Fluorescent/colorimetric Chemical Sensor Array), Task 2.3 (Optimization of The Colorimetric/Fluorescent Chemical Sensor Array and Its Corresponding Network), and Task 3 (Integration of Corrosive Water into Internal Corrosion Prediction Models). The detail findings are described as below:

1. Background and Objectives in the 6th Quarter

1.1 Background

This project is designed to develop passive colorimetric/fluorescent chemical sensor array for locating and detecting corrosive water inside pipes. Inside the pipelines, the transported crude oil may include a hot mixture of free water, carbon dioxide (CO_2), hydrogen sulfide (H_2S) and microorganisms. The different chemical components inside oil/water environment such as HCO_3^- / CO_3^{2-}, Fe^{3+}, S^{2-}, H^+ or pH may result in different internal corrosion mechanisms, such as sweet corrosion or sour corrosion. The passive colorimetric sensor array to be developed in this project is intended to detect the concentration changes of the five above mentioned important chemical species in the internal oil/water environment of the pipeline and use these detected environmental data to predict the internal corrosion progressing of pipelines.

1.2 Objectives in the 6^h Quarter

In this quarter, we will write the S^{2-} and H^+ sensors in the CA/PMMA film, which were proved effective under mechanical friction environment in last quarter. More importantly, the sensitivity tests on the Fe^{3+}, S^{2-}, and Fe^{2+} ions also will be tested to quantify the color changes and form a base of establishing corrosion model according to the sensors' responses to target components in pipelines. In addition, for the stress analysis under cleaning activities, a sensitivity test on the influence of membrane thickness is needed to provide a deep view of thickness optimization. Also, the corrosion model for analyze the effect of S^{2-} concentration will be discussed.

2. Results and Discussions

2.1 Development of Fluorescent/Colorimetric Chemical Sensor Array (Task 2.1)

In this quarter, we did the planned study on selecting and testing CA/PMMA film with embedded sensors for detecting S^{2-} and H^+ ions. The results showed that in addition to Fe^{2+}/CO_3^{2-} and Fe^{3+}, the detection of S^{2-} was successfully using CA/PMMA polymer films with embedded sensors. The sensor embedment of H^+ ions is also completed. Sensing tests on the embedded H^+ ions will be tested in next quarter.

2.1.1 CA/PMMA film with embedded sensors for detecting S^{2-} and H^+ ions (Task 2.1)

2.1.1.1 Preparation of the CA/PMMA film and S^{2-} sensor embedment

Cellulose acetate (CA) (0.5 g) was dissolved in DMF (3.7 g) and hexane (2 g) at 85 °C for 5 h to form a homogeneous casting solution. In the meantime, Poly(methyl methacrylate) (PMMA) (0.5 g) was dissolved in THF (4 mL) and the PMMA solution was stirred at room temperature for 5 h to form the polymer solution completely. Then, these polymer solutions were mixed and stirred at 85 ^{o}C for 1 h to

form a homogenous phase. Two sensor doping concentrations were tested including 20% and 10% sensor to polymer ratios. For 20% sensor doping concentration, 224 mg Cu_2Cl_2-phenanthroline complex was added as sensor to the CA/PMMA polymer solution; and for the 10% sensor doping concentration, 112 mg Cu_2Cl_2-phenanthroline complex was added as sensor to the CA/PMMA polymer solution. The solution with sensors was then stirred for 30 min at 85 ^oC. A thin film was cast on a glass plate inside a hot chamber at 85 °C for 1 h. The film was covered by a glass container and left at room temperature. The film was immersed in a room-temperature DI water coagulation bath until it was detached. The film was then taken out and kept in another fresh DI water for 48 h to remove any trace of solvent. The wet film was used directly for the tests.

Fig.1. Photo of Cu_2Cl_2-phenanthroline sensor in CA/PMMA film for S^{2-} detection

2.1.1.2 Sensitivity tests on detecting S^{2-} ions

The prepared CA/PMMA film with embedded S^{2-} sensors of two different sensor concentrations including 20% and 10% sensor to polymer ratio, were cut into small segments and tested in different Na_2S aqueous solution from 1 % to 0.05 %, with ten different S^{2-} concentrations of 1%, 0.9%, 0.8%, 0.7%, 0.6%, 0.5%, 0.4%, 0.3%, 0.2%, 0.1%, 0.075%, and 0.05 %. The small test segments were soaked in the Na_2S aqueous solution with the ten different concentrations for 7 days and were taken out and washed with water to observe color change. Fig. 2 shows the detail procedure and photos of sensitivity test scene and results for the sensor doping concentration 20% (sensor to polymer ratio). It can be seen clearly that at 20 hours, some black spots appeared on the surface of the film. The reaction between the embedded sensor and the S^{2-} ion turned the color of the sensor film to black color and as the increase of the concentration of the S^{2-} ion, the color of the sensor film turns darker. Fig. 2 also shows that the sensor film has an obvious color change for S^{2-} concentration of 0.05%. The resolution of the sensor film for S^{2-} detection is higher than 0.05% concentration. However, when the sensor film was washed by ultrasonic in deionized water, part of the black solid in the film fall off and dissolved in the water. Therefore, with 20% of sensor doping concentration, copper sulfide does not adhere to the film surface easily in the flowing liquid as in the oil/gas pipeline inner surface. Thus, sensitivity tests were also performed on the 10% sensor doping

concentration to see if the concentration of the sensor doping would influence the survivability of the sensor film.

film

Impregnate in a solution of the corresponding concentration

Na_2S solution:

Film in the ion solution at 0 day

Film in the ion solution at 20 hours

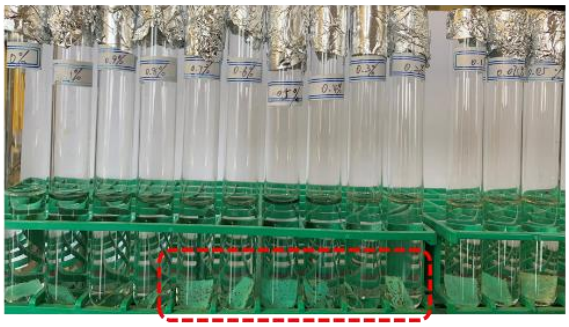

Film in the ion solution at 7 days

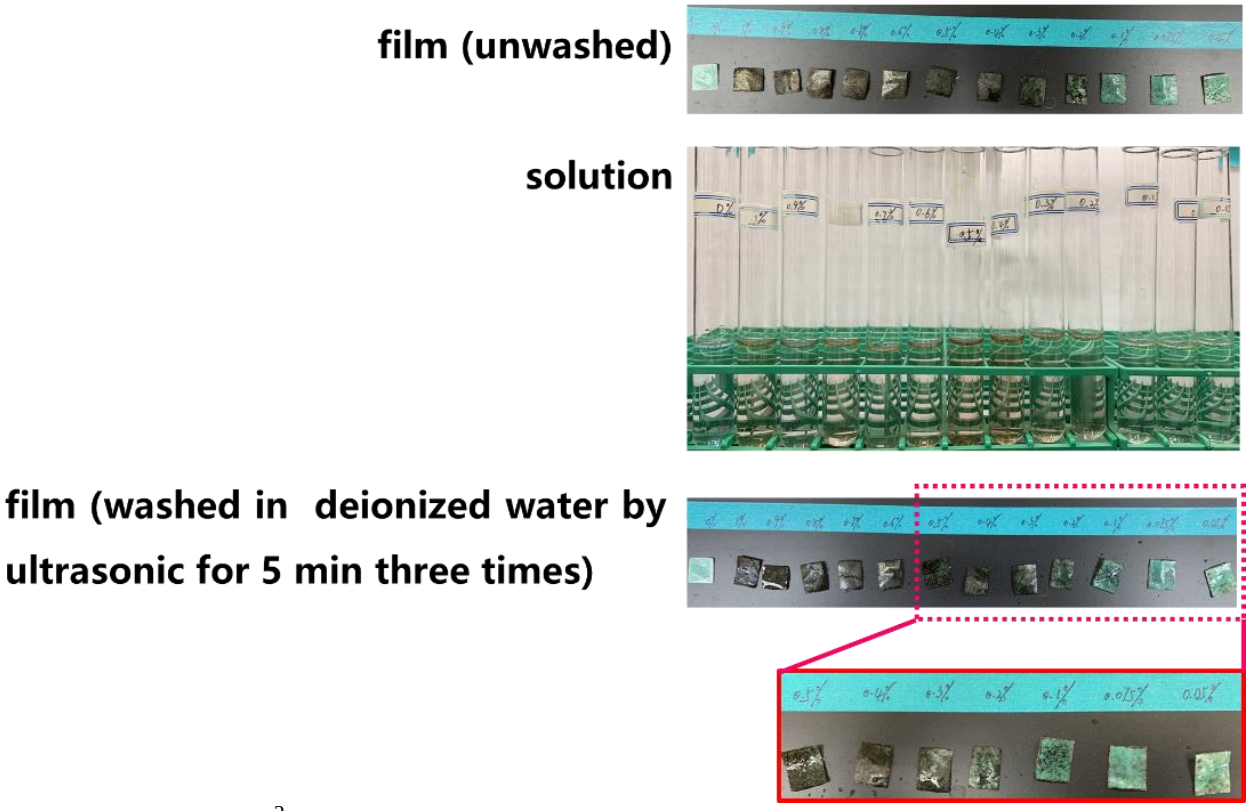

Fig. 2. S^{2-} sensitivity testing for sensor doping concentration 20%

Fig. 3 shows the detail procedure and photos of sensitivity test scene and results for the sensor doping concentration 10% (sensor to polymer ratio). It can be seen clearly that at 2 days, some black spots appeared on the surface of the film. The reaction between the embedded sensor and the S^{2-} ion turned the color of the sensor film to brown color and as the increase of the concentration of the S2- ion, the color of the sensor film turns darker. Fig. 3 also shows that the sensor film has an obvious color change for S^{2-} concentration of 0.05%. The resolution of the sensor film for S^{2-} detection is higher than 0.05% concentration. When the film was washed by ultrasonic in deionized water, the brown solid generated by the reaction between the embedded sensor and the S^{2-} ion in the film didn't fall off obviously. The brown solid can be absorbed in the film at the sensor doping concentration of 10 %. Therefore, a sensor doping concentration of 10% is recommended for the detection of S^{2-} ions on the oil/gas pipeline inner surface. In the future color quantification, 10% sensor doping concentration is applied.

film

Impregnate in a solution of the corresponding concentration

Na_2S solution:

Film in the ion solution at 0 day

Film in the ion solution at 2 days

Slight black

Film in the ion solution at 7 days

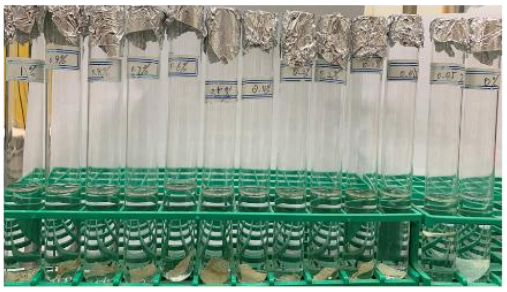

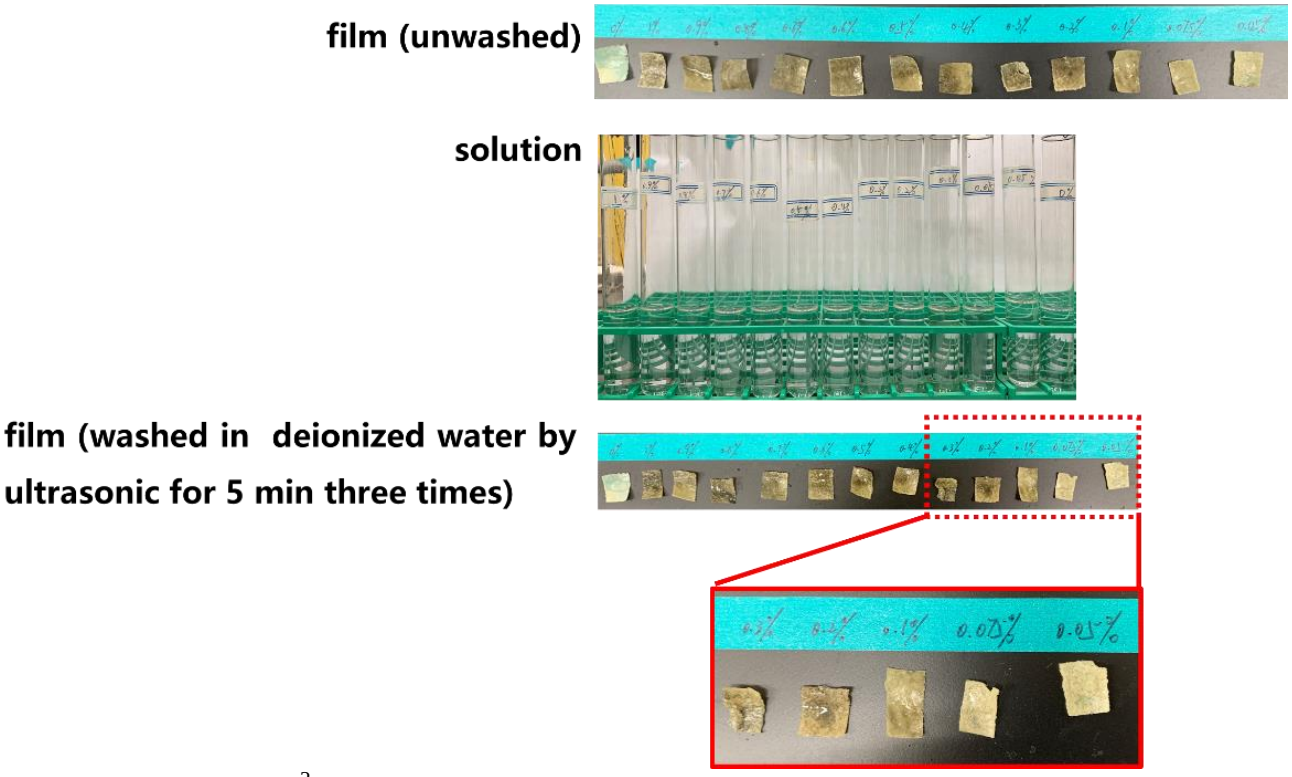

Fig. 3. S^{2-} sensitivity testing for sensor doping concentration 10%

2.1.1.3 Preparation of the CA/PMMA film and H^+ sensor embedment

In this quarter, the team also made some CA/PMMA films with H^+ sensor embedded. The CA/PMMA film was prepared using the same procedure as for the S^{2-} sensor. Cellulose acetate (CA) (0.5 g) was dissolved in DMF (3.7 g) and hexane (2 g) at 85 °C for 5 h to form a homogeneous casting solution. In the meantime, Poly(methyl methacrylate) (PMMA) (0.5 g) was dissolved in THF (4 mL) and the PMMA solution was stirred at room temperature for 5 h to form the polymer solution completely. Then, these polymer solutions were mixed and stirred at 85 ^oC for 1 h to form a homogenous phase.

After the preparation of the CA/PMMA polymer solution, 250 mg Schiff-base H^+ sensor was added into the polymer solution. The solution was stirred for 30 min at 85 ^oC. A thin film was cast on a glass plate inside a hot chamber at 85 °C for 1 h. The film was covered by a glass container and left at room temperature. The film was immersed in a room-temperature DI water coagulation bath until it was detached. The film was then taken out and kept in another fresh DI water for 48 h to remove any trace of solvent. In this process, the color of film changed from pale-yellow to brown as seen in Fig. 4. The water in lab may be not the DI water. A large amount of Fe^{3+} was existence. Thus, we will prepare some more CA/PMMA films with H^+ sensors next quarter to fix this problem and test its sensitivity with H^+ concentration changes.

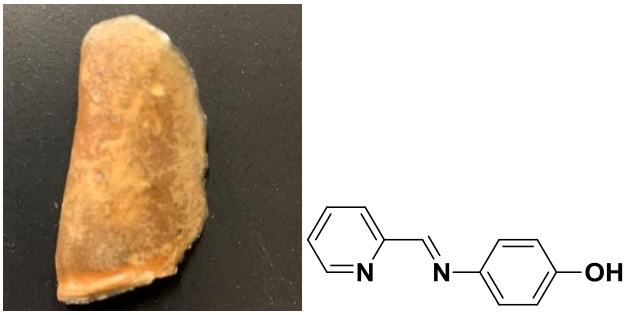

Fig.4. Photo of Schiff-base sensor CA/PMMA film for H^+ sensing

2.2 Calibration of the Fluorescent/colorimetric Chemical Sensor Array (Task 2.2)

With a successful S^{2-} sensor in the CA/PMMA film, in this quarter, we also performed a detailed sensitivity test on the developed sensors for detecting the Fe^{3+}, S^{2-}, and Fe^{2+} ions. To quantify the color changes using numerical numbers, a colorimetry system based on International Commission on Illumination (abbreviated as CIE from its French title) standard will be developed for the developed sensor array with experimental inputs from the laboratory sensitivity analysis for the concentration changes of the Fe^{3+} and S^{2-} ions. In next quarter, we will continue correlate the color changes to numerical matrix for color detection for both Fe^{3+} and S^{2-} ions and also quantify the color changes of Fe^{2+} ions.

2.2.1. CIE Based Colorimetry System

To identify a color with an absolute value, in this quarter, a standard colorimetry system was developed based on the recognition mechanism of human eyes. [1, 2] The cone cells in the human eye are natural sensors responsible for color vision. Previous researches with detailed experimental results determined that the 6 to 7 million cone cells in human eyes can be divided into 3 main perceptual categories, which correspond to red, green, and blue, respectively, as shown in Fig. 5. About 65% of cone cells are specialized sensitive to red light, while 33% are sensitive to green light, and only 2% are sensitive to blue light (but the sensitivity strength of blue light is much stronger that the other two categories).

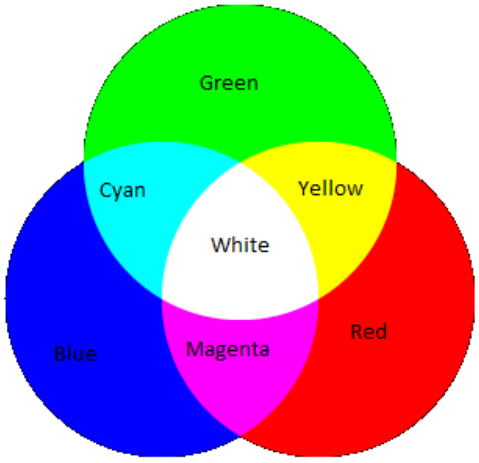

Fig. 5. Three primary colors

International Commission on Illumination (abbreviated as CIE from its French title) stipulates that the wavelengths of the three primary colors of red, green and blue are 700nm, 546.1nm, and 435.8nm, respectively (Fig. 5). In the color matching experiment, when the relative brightness ratio of the three primary colors is 1.000: 4.5907: 0.0601, they can be matched the equivalent white light. Thus, CIE chooses this ratio as the unit quantity of the three primary colors of red, green and blue, namely

(R):(G):(B)=1:1:1. Although the brightness values of the three primary colors are not equal with each other, CIE treats the brightness value of each primary color as a unit. Therefore, the relationship of red, green, and blue color with 1-unit strength can be written as Eq.1:

$$(R)+(G)+(B)=(W). \quad (1)$$

When the ratio of the three-fundamental color changes, different color of light witch has different wavelength can be achieved. The corresponding test method is called color matching, and the amount of each color of red, green and blue by unit is called tristimulus value. To a certain color with a certain wavelength, the matching equation can be expressed as Eq.2:

$$C_o = R(R) + G(G) + B(B) \quad (2)$$

In the formula, C represents the color to be matched; (R), (G), and (B) represent the unit quantities of the three primary colors of red, green, and blue which are mentioned above; R, G, and B are the red, green and blue colors required to match the color to be matched, which are tristimulus values; and "o" means visually equal, that is, color matching.

By using this method, any visible color or light can be described as a mixing of the identified RGB color. To determine the RGB tristimulus values of the visible light, CIE introduced CIE-RGB tristimulus values (Table.1) for the light with wavelength range from 380nm to 780nm.

Table 1. CIE-RGB tristimulus values

WAVELENGTH (NM)	$\bar{r}$	$\bar{g}$	$\bar{b}$
380	0.00003	-0.00001	0.00117
400	0.00030	-0.00014	0.01214
420	0.00211	-0.00110	0.11541
440	-0.00261	0.00149	0.31228
460	-0.02608	0.01485	0.29821
480	-0.04939	0.03914	0.14494
500	-0.07173	0.08536	0.04776
520	-0.09264	0.17468	0.01221
540	-0.03152	0.21466	0.00146
560	0.09060	0.19702	-0.00130
580	0.24526	0.13610	-0.00108
600	0.34429	0.06246	-0.00049
620	0.29708	0.01828	-0.00015

640	0.15968	0.00334	-0.00003
660	0.05932	0.00037	0.00000
680	0.01687	0.00003	0.00000
700	0.00410	0.00000	0.00000
720	0.00105	0.00000	0.00000
740	0.00025	0.00000	0.00000
760	0.00006	0.00000	0.00000
780	0.00000	0.00000	0.00000

This CIE-RGB spectrum tristimulus value is obtained by 317 normal vision people using the three primary colors of red, green, and blue specified by CIE. During the experiment, the number of red, green, and blue primary colors corresponding to the isoenergetic spectral color of each wavelength of the matching spectrum is the spectral tristimulus value, which is tested as $\overline{r}\,\overline{g}\,\overline{b}$. As can be seen from Table 1, the spectral tristimulus value is negative in many cases. This is because the color to be matched is monochromatic light with high saturation, and the saturation of the three primary color lights must be reduced after mixing, resulting in a failure to match the color to be matched. In order to achieve color matching, one of the three primary color lights on the upper red, green, and blue sides must be moved to the negative side to be matched in the experiment.

In order to intuitively represent the proportion of the three primary colors (RGB), chromaticity coordinates were introduced as functions as r, g, b, which is shown in Eq.3:

$$\begin{aligned} r &= R/(R+G+B) \\ g &= G/(R+G+B) \\ b &= B/(R+G+B) \end{aligned} \tag{3}$$

where, it is known that r+g+b=1. When using the tested spectral tristimulus value, Eq.3 can be written as Eq.4,

$$\begin{aligned} r &= \bar{r}/(\bar{r}+\bar{g}+\bar{b}) \\ g &= \bar{g}/(\bar{r}+\bar{g}+\bar{b}) \\ b &= \bar{b}/(\bar{r}+\bar{g}+\bar{b}) \end{aligned} \tag{4}$$

where, r, g, and b are the chromaticity coordinates to describe a certain light. By using the tested value of red (R) and green (G) light in Table 1, a flat-horseshoe-shaped figure can be obtained as shown in Fig. 6, which is called the CIE-RG chromaticity diagram.

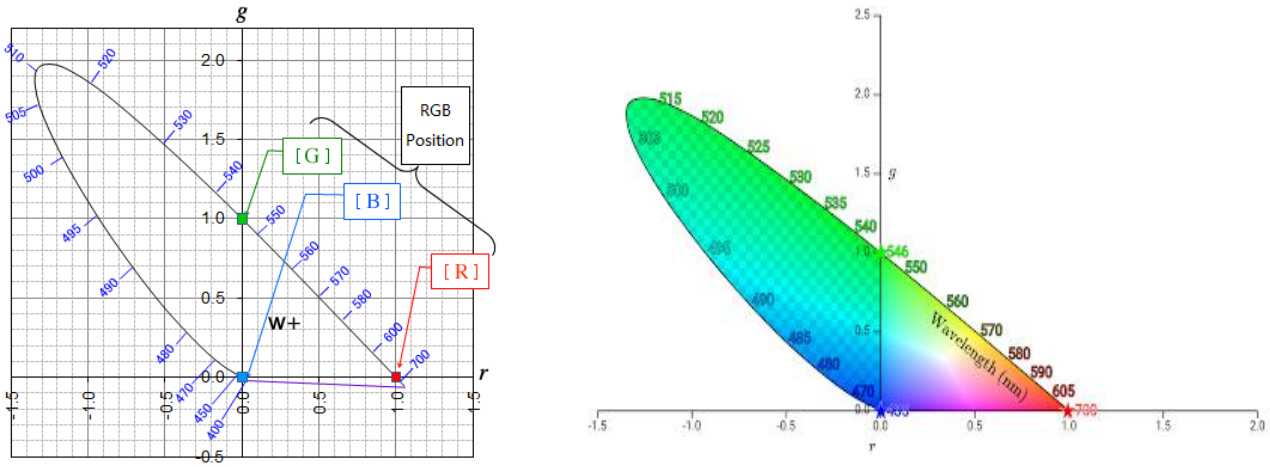

Fig. 6. CIE-RG chromaticity diagram

The CIE color quantification system exampled in Fig. 6 specifies isoenergetic white light (color temperature 5500K), which is located in the center of the chromaticity diagram (0.33, 0.33). In the CIE-RG chromaticity diagram, the chromaticity coordinates reflect the relative proportions of the three primary colors in the total tristimulus value. A set of chromaticity coordinates represents the common characteristics of those colors with the same hue and same saturation but different brightness. Therefore, the CIE-RG chromaticity diagram does not reflect the change of color brightness, but only expresses the range of color gamut. The spectral tristimulus value of the CIE-RG system can be obtained from experiments. It can be used for color measurement and calibration and chromaticity calculation. However, the negative portion of the diagram had made it inconvenient and unintelligible for practical use. Therefore, in 1931, CIE recommended a new international colorimetric system, namely CIE-xyz system, which is also known as the xyz international coordinate system [3].

For the CIE-xyz system as shown in Fig. 7 for its chromaticity diagram, it uses mathematical methods to select three ideal primary colors instead of the actual three primary colors, so that the spectral tristimulus values and chromaticity coordinates r, g, and b in the CIE-RG system become positive. The location of the selected ideal colors in Fig. 7 is shown in Table. 2, where X, Y, Z represent the red, green and blue primary color ideally. After mathematical transformation, the relationship of the two-color systems and the two coordinate systems are shown in Eq. 5 and Eq. 6, respectively:

$$\begin{aligned} X &= 0.490R + 0.310G + 0.200B \\ Y &= 0.177R + 0.812G + 0.011B \\ Z &= 0.010G + 0.990B \end{aligned} \tag{5}$$

where X, Y, Z are the new ideal colors, R, G, B are the identified color of red, green and blue.

$$\begin{aligned} x &= (0.490r + 0.310g + 0.200b)/(0.667r + 1.132g + 1.200b) \\ y &= (0.117r + 0.812g + 0.010b)/(0.667r + 1.132g + 1.200b) \\ z &= (0.000r + 0.010g + 0.990b)/(0.667r + 1.132g + 1.200b) \end{aligned} \tag{6}$$

in which, x, y, z are the coordinates in the CIE-xyz system, while r, g, and b are coordinates of CIE-RG system [4].

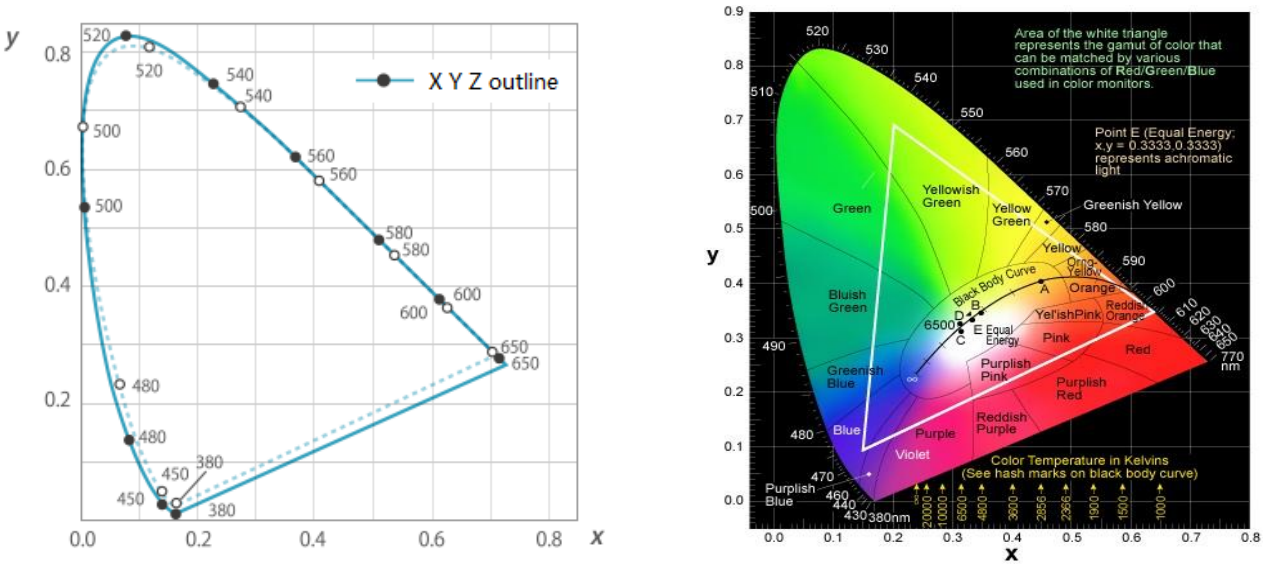

Fig. 7. CIE-Yxyz chromaticity diagram

Table 2. RGB value of ideal colors of X, Y, Z

	R	g	b
X	1.275	-0.278	0.003
Y	-1.739	2.767	-0.028
Z	-0.743	0.141	1.602

Therefore, as long as the chromaticity coordinates r, g, and b of a certain color are known, we can find their chromaticity coordinates x, y, and z in the newly identified three primary colors xyz color space. Through the transformation of Eq. 5, for spectral colors or all the natural colors, the transformed chromaticity coordinates are all positive values. While the chromaticity coordinates of isoenergetic white light remain unchanged as (0.33, 0.33), Table 3 is the results calculated by the CIE-Yxyz system according to the data in Table 1 and using Eq. 6. It shows that all the values of the spectral chromaticity coordinates x, y, and z are positive values. The recalculated color location in CIE-Yxyz system and the corresponding diagram is shown in Fig. 7, which is the most commonly used chromaticity diagram in academic researches nowadays.

Table 3. CIE-xyz tristimulus values

WAVELENGTH (NM)	X	Y	Z
380	0.1741	0.0050	0.8209
400	0.1733	0.0048	0.8219
420	0.1714	0.0051	0.8235
440	0.1644	0.0109	0.8247

460	0.1440	0.0297	0.8263
480	0.0913	0.1327	0.7760
500	0.0082	0.5384	0.4534
520	0.0743	0.8338	0.0919
540	0.2296	0.7543	0.0161
560	0.3731	0.6245	0.0024
580	0.5125	0.4866	0.0009
600	0.6270	0.3725	0.0005
620	0.6915	0.3083	0.0002
640	0.7219	0.2809	0.0001
660	0.7300	0.2700	0.0000
680	0.7334	0.2666	0.0000
700	0.7347	0.2653	0.0000
720	0.7347	0.2653	0.0000
740	0.7347	0.2653	0.0000
760	0.7347	0.2653	0.0000
780	0.7347	0.2653	0.0000

From Table 3, it can be seen that all the value become positive and the sum of x, y, z is equal to 1. In the CIE-Yxyz diagram as seen in Fig. 7, each color with a certain portion of three priority colors can be expressed as a function of x and y. However, the ability of distinguish the brightness demand for further improvement on the three-dimensional space by introducing brightness factor Y, which refers to the CIE-Yxyz chromaticity diagram.

In theory, the color change of the tested sensors in different cases should have a corresponding path on the diagram. Technically, as long as the color change is recognizable by electronic devices, a translation system, which is based on the chromaticity diagram, is applicable to convert the information into concentration of specific ions the sensors contact. The sensitivity tests performed in this quarter will provide this quantification system based on this principle.

In the CIE-Yxyz chromaticity diagram shown in Fig. 7, the x chromaticity coordinates correspond to the ratio of the red primary color, and the y chromaticity coordinates correspond to the ratio of the green primary color. From the position of each wavelength of the horseshoe-shaped spectral trace in the figure, it can be seen that the red band of the spectrum is located at the lower right of the graph, the green band is located at the upper part of the graph, and the blue band is located at the lower left of the graph. The white point E in the center has the lowest saturation and the highest saturation on the light source trace. If the

wavelength points representing different colors of light on the spectral track are connected to the white light point in the center of the chromaticity diagram, the chromaticity picture can be divided into various different color regions. Therefore, if the chromaticity coordinates x, y of a color can be calculated, its color characteristics can be clearly determined in chromaticity. For example, the chromaticity coordinates of the cyan sample are x = 0.1902 and y = 0.2302. However, the chromaticity coordinates only specify the chromaticity of the color, but not the brightness of the color, so if a unique value is demanded for a certain color, we must also indicate its brightness characteristics, which is the size of Y. It describes the intensity of light reflected by an object as a percentage of the light of the light source. Thus, Y has a value from 0-100. In this way, with both the chromaticity coordinates x and y representing the color characteristics and the brightness factor Y representing the color brightness characteristics, the appearance of the color can be completely and uniquely determined.

2.2.2 Sensor Sensitivity Test and Color Change Quantification for Fe^{3+} Ions

In the last two quarters, the sensing tests of Fe^{3+} ions have been performed and reported. The PMMA/CA films with embedded phenanthroline sensor showed significant color changes with Fe^{3+} ion ranging from 0%, 0.1%, 1%, and 5%. However, the concentration of Fe^{3+} ions under lab condition is for the confirmatory test. To reveal the colorimetric response to a certain concentration of Fe^{3+} ion, sensitivity tests of Fe^{3+} irons have been conducted in this quarter. To correlate the sensor's colorimetric response to the indication of Fe^{3+} concentration, sensing tests were conducted with Fe^{3+} solution ranging from 0.05% to 1% which covers the empirical concentration under inline condition. After the fabrication of the PMMA/CA film, the segments were immersed in ion solutions for at least one week to observe the color change. The test procedure and polymer segments are shown in Fig. 8.

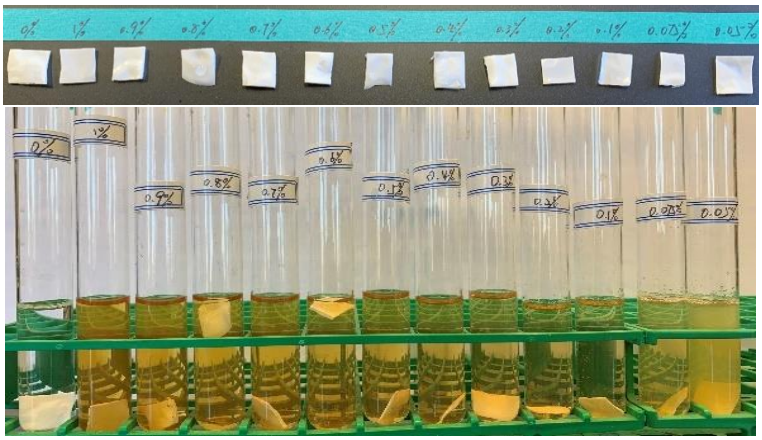

Fig. 8. Test segments

In the preparation of polymer membranes, exactly the same procedure was repeated as indicated in Section 2.2.1 with 500 mg phenanthroline Fe^{3+} sensor was added in the CA/PMMA polymer solution. Thirteen polymer segments with 1mm thickness were fabricated to be immersed in $FeCl_3$ solutions with concentration level 0.05%, 0.075%, 0.1%, 0.2%, 0.3%, 0.4%, 0.5%, 0.6%, 0.7%, 0.8%, 0.9%, 1.0% from low to high. The detail test procedure and test results are shown in Fig. 9. After 7 days of immersing, the sensors showed significant color change responding to the existence of Fe^{3+} ions. As shown in the segments outlook, as the concentration increases, the deposit color turns heavier from light pink to red. This trend illustrates a promising indication of the ion concentration to the color appearance. However, by simply checking the color change of the polymer membranes, it is hard to tell the precise concentration of the tested ions. To have a more detailed view of the color change towards the Fe^{3+} ions, sensitivity analysis is performed using the developed colorimetry methods mentioned in last section.

film

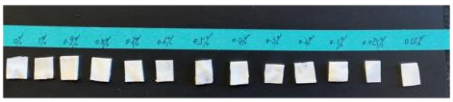

Impregnate in a solution of the corresponding concentration

$FeCl_3$ solution:

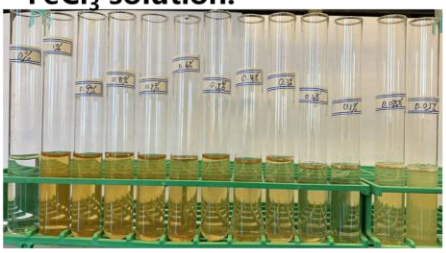

Film in the ion solution at 0 day

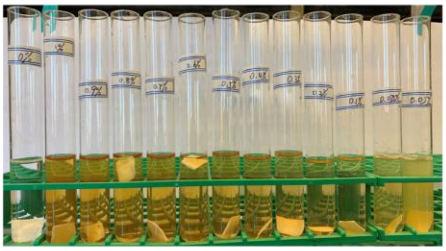

Film in the ion solution at 20 hours

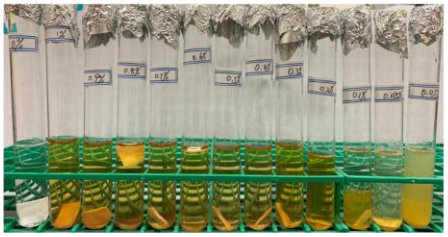

Film in the ion solution at 7 days

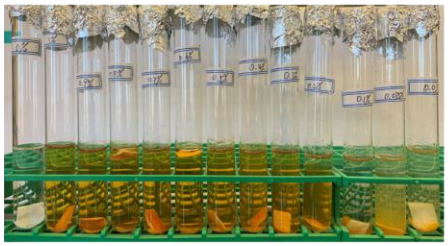

film (unwashed)

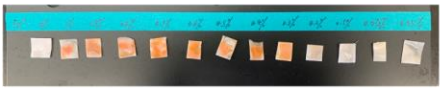

solution

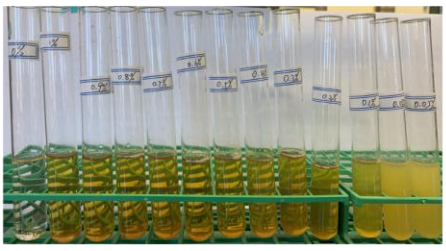

film (washed in deionized water by ultrasonic for 5 min three times)

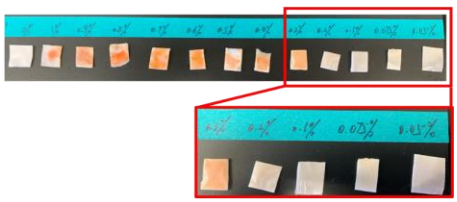

2.2.3 Sensor Sensitivity Test for Fe^{2+} ion

Sensitivity tests were also performed on the Fe^{2+} ion. The CA/PMMA polymer solution as indicated in Section 2.2.1, for Fe^{2+} ion detection, 500 mg phenanthroline Fe^{2+} sensor was added. All other procedure followed the same as described in Section 2.2.1. The CA/PMMA sensor film was then immersed in the $FeCl_2$ solutions with concentration level 0.05%, 0.075%, 0.1%, 0.2%, 0.3%, 0.4%, 0.5%, 0.6%, 0.7%, 0.8%, 0.9%, 1.0% from low to high as shown in Fig. 10. As seen in Fig. 10, similar as for Fe^{3+} detection, the color change is very consistent. A higher Fe^{3+} ion concentration results in a heavier red color. Also, the sensor film can detect 0.05% concentration of the Fe^{3+} ions well, indicating a resolution higher than 0.05%. In next quarter, color quantification will also be performed on Fe^{3+} detection as for the Fe^{2+} ions.

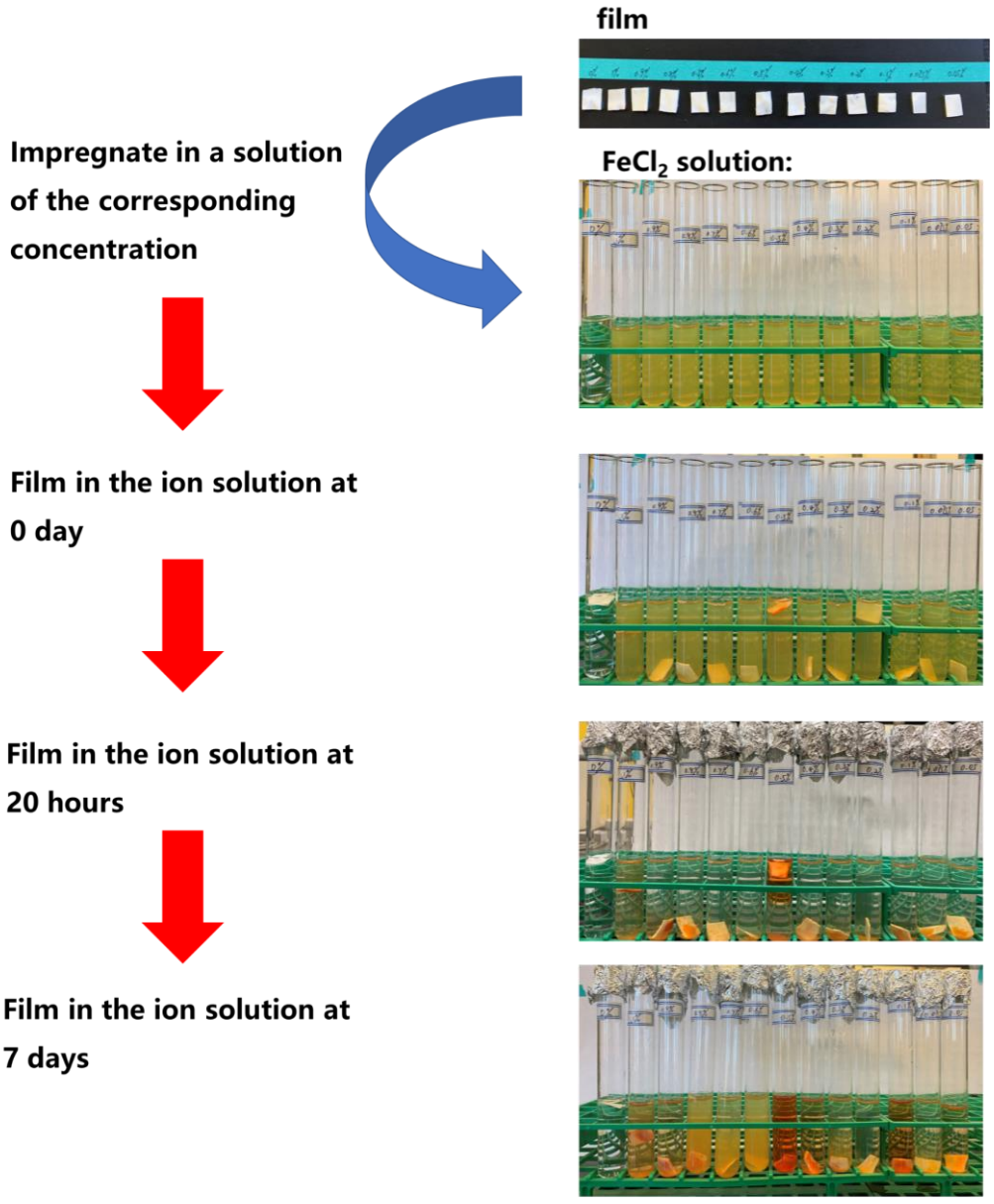

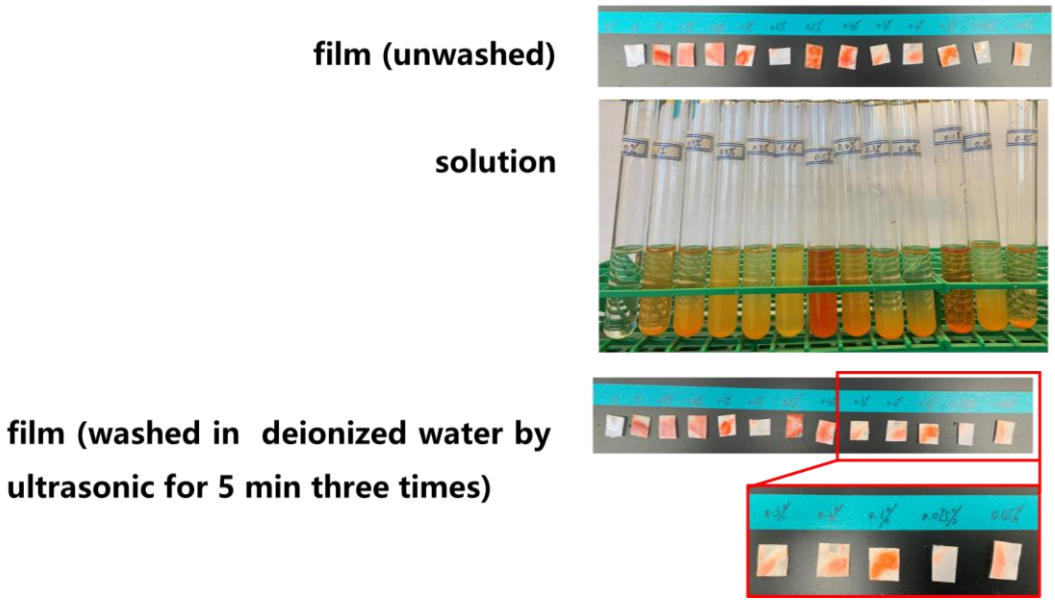

Fig. 10. Sensitivity tests on Fe^{2+} detection

2.2.4 Optimizing Sensor Thickness based on Sensor's Survivability under Oil Condition (Task 2.3)

It is known from our previous reports that during the regular cleaning activities, the mechanical pressure on the sensor is sensitive to its thickness. For safety and durability considerations, we further measure the relationship between the sensor thickness and the pressure on the basis of previous research in order to optimize the thickness of the sensor, which is the thickness sensitivity test. The brief test layout used the same devices and specimens is shown in Fig. 11.

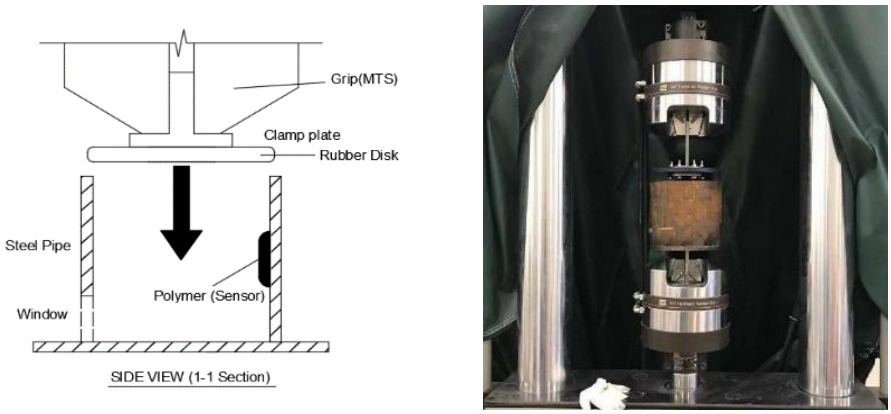

Fig. 11. Test layout

After the designed test procedure, a representative displacement-load curve is shown in Fig. 12. The test procedure is divided into two stages, which are cleaning devices moving in and out. When the disk goes in, the rubber needs to be squeezed and driven into the pipe, so that the curve peaks with a rapid increase of load. After the disk is fully pushed into the pipe, the rubber bounced back to release a small amount of load, so that the curve shows a sudden drop and followed by a gradual increase and then becomes steady. At the steady stage of the curve, it is reckoned as the average friction between the disk and the pipe's inner surface where the sensors vary in thickness attached. The average load of the 1mm-sensor case is shown in Fig. 12.

Obviously, the value of the average friction load increases with the thickening of sensors, because the sensors are obstacles which block the running of rubber. Considering transfer the load into stress in

polymer membranes, a conversion relationship is established for verification purpose of the two approaches. With the assumption that the contacting area of the disk and the pipe was a circular ring, the shear stress could be calculated by Eq. (7) in which *F* is Axial load given by the experimental tests:

$$\tau_{sensor} = \frac{F}{A_r} \tag{7}$$

where, *F is the* axial load of experimental results, and A_r *is the* area of the contacting area which can be calculated as below:

$$A_r = l \times d \tag{8}$$

where, *l* is the contacting length between the disk and the sensor, and *d* is its width.

In the thickness sensitivity test, a 2 mm contacting width used from the simulation result (mesh dimension of the rubber disk was 1 mm/cube) and a 15mm length measured in experimental tests were adopted to calculate the corresponding stress. The experimental tests in the previous report indicated that 540 N load was measured when disk went through the pipe without sensors. Combining with the tested load in Fig. 10, which is 592 N, 52 N of the axial load was induced by the presence of sensor. This means the sensor carried a force of 52 N when the disk passed through the sensor. The size of the brushed polymer membrane is 25.4mm×25.4mm (1"×1") and the tested data of sensors from 0mm to 6mm thick with an increment of 0.25mm (minimum thickness of brushed layer) are shown in Fig. 13.

From Figs. (12, 13), we know that the stress induced by friction in polymer membrane soars rapidly in two sections, which is 0.5mm to 2mm and over 3.5mm. So, for the survivability concern, the recommended thickness of the sensor base is less than 3.5mm, so that the stress in sensor can be controlled below 2.56 Mpa.

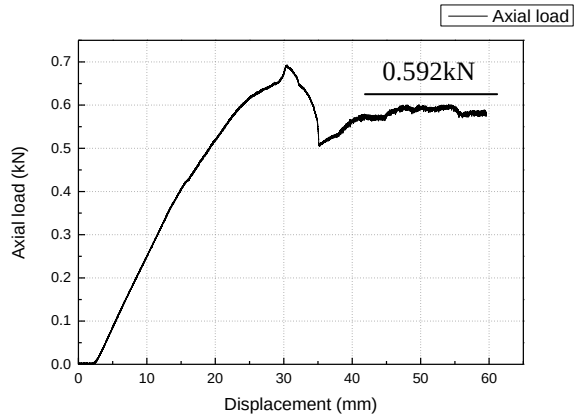

(a) Load-Displacement curve of In-stage

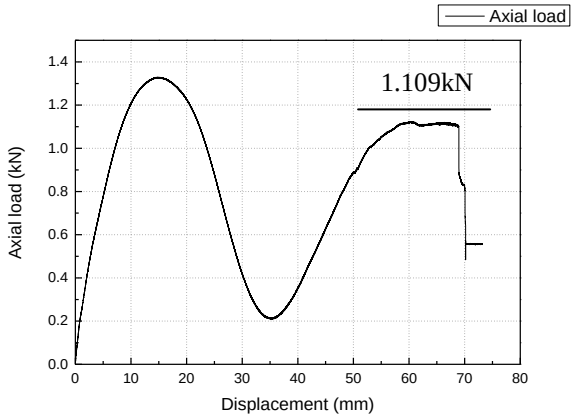

(d) Load-Displacement curve of Out-stage

Fig. 12. Load-displacement curve

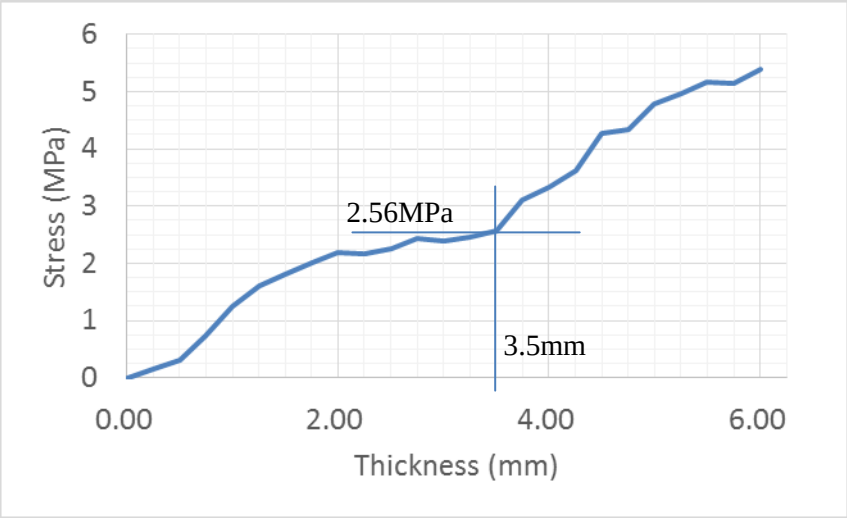

Fig. 13. Stress-Thickness curve of polymer membranes

2.2.5 Integration of Corrosive Water into Internal Corrosion Prediction Models (Task 3)

To establish the relationship between corrosion environments and the prediction models, numerical and mechanistic models will be introduced in this project. From the previous report, the Johnson and Tomson (JT) model (Eq. 9.) was selected to corelate Corrosion Rate (CR) with the concentration of CO_3^{2-} and Fe^{2+} under pipeline environment. [5]

$$R_{FeCO_3} = A \times e^{54.8-\frac{128.0kJ/mol}{RT}} \times K_{sp} \times (S^{\frac{1}{2}} - 1)^2 \quad (9)$$

According to van Hunnik, et al., the expression of JT model can be modified as:

$$R_{FeCO_3} = A \times e^{52.4-\frac{119.8kJ/mol}{RT}} \times K_{sp} \times (S-1)(1-S^{-1}) \quad (10)$$

In these two expressions (9, 10), *A* is the surface area available for precipitation per unit volume and K_{sp} is the precipitation rate constant, *R* is Boltzmann constant, and *S* represents the considerable supersaturation of Fe^{2+} or CO_3^{2-} ($S = c_{Fe^{2+}}$ *or* $c_{CO_3^{2-}}/K_{sp}$), where $c_{Fe^{2+}}$and $c_{CO_3^{2-}}$ are the tested concentration of, Fe^{2+} and CO_3^{2} respectively. The solubility product (K_{sp}) for $FeCO_3$ is constant and modeled as a function of temperature (°C).

To find a similar model to correlate corrosion with the existence of sulfur (S^{2-}) ions, corresponding literature review has been done in this quarter. Comparing with the model on other ions, the studies of sulfur's impact in corrosion is rarely posted. In 1996, J. H. Wang et. al [6] conducted research on atmospheric corrosion modeling in steel under sulfur dioxide-polluted environment. It indicated that Sulfur dioxide (SO_2) is always the most important pollutant in an industrial atmosphere. SO_2 absorbed in the moisture is believed to form sulfurous acid (H_2SO_3) initially and sulfuric acid (H_2SO_4) after atmospheric oxidation. H_2SO_4 absorbed by rust continues to accelerate corrosion.

To get data demanded in establishing corrosion model, experimental tests were conducted by using accelerated corrosion test was adopted, in which an electrochemical cell in Fig. 14 was built as test specimen to be exposed under test cases. In this specimen, a working electrode WE of steel was embedded vertically in an acrylic resin cell. This cell consisted of two WE, one reference electrode (RE, platinum ring 0.3 mm), and one counter electrode (CE, platinum rod 2 mm). The CE was at the center of the cell, and the RE was outside the cell. The distance between the WE and the CE was ~2 mm. The electrochemical cell was also exposed to the accelerated corrosion testing environment in the test chamber. A thin electrolyte layer was formed by dropping distilled water on the surface of the specimens

before introducing SO_2 into the chamber. The thickness of the water layer on the cell surface was ~0.3 mm as measured by the weight of the electrolyte layer. Impedance measurements carried out on the electrochemical cell were initiated only after 4 h of SO_2 addition during each wetting period. Both the platinum electrode potential and WE potential were steady thereafter. Impedance measurements were taken using a frequency response analyzer. The amplitude of the sinusoidal signal was 10 mV, close to the open circuit potential. The frequency ranged from 100 kHz to several mHz. Analysis of impedance data was performed using the computer analysis program. And the weight-loss measurements were made after various exposure periods. Corrosion products on the specimens were removed chemically by immersion in Clark's Solution (CS). Atmospheric corrosion of CS in the natural exposure test and the accelerated test followed the Bilogarithmic equation (Eq. 11):

$$C = At^B \tag{11}$$

where C is the weight loss recalculated in terms of thickness loss (μm), t is the exposure time (month or test cycle), and A and B are constants. A is equivalent to weight loss when time is unity and, therefore, is considered as a measure of the initial corrosion resistance of metals. B reflects the change of weight loss with exposure time.

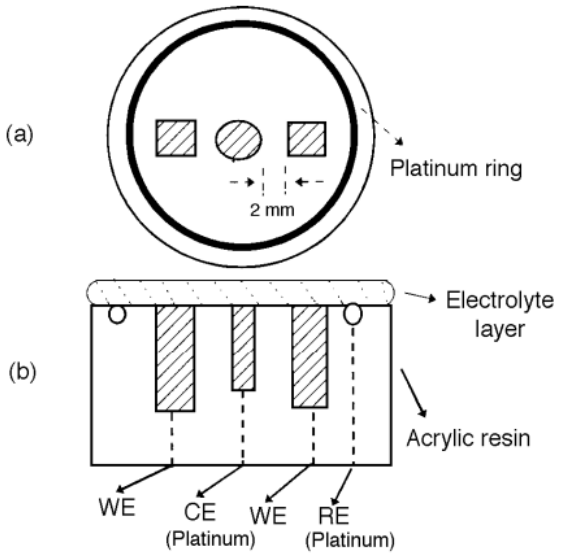

Fig. 14. Test specimen for recyclable use

The reaction mechanism was described as, in the presence of SO_2, it is likely that SO_2 first is adsorbed on rust and oxidized afterward to sulfate (SO_4^{2-}) according to:

$$SO_2 + O_2 + 2e^- = SO_4^{2-} . \tag{12}$$

The electrons come from the reaction:

$$Fe(OH)_2 = FeOOH + H^+ + e^- \tag{13}$$

or from the anodic dissolution of iron:

$$Fe = Fe^{2+} + 2e^- \tag{14}$$

SO_4^{2-} in the thin electrolyte layer interferes with the Fe(OH) species according to the process proposed by Barton and Bartonova [7]

$$Fe(OH)_x + SO_4^{2-} = FeSO_4 + OH^- + e^- \tag{15}$$

After the determination of the reaction mechanism favored in this study, certain cycles of forming and

deforming of sulfur films were conducted with the measurement of corrosion rate (weight loss), and by fitting the curve, 3 corrosion models were concluded as shown in Fig. 15.

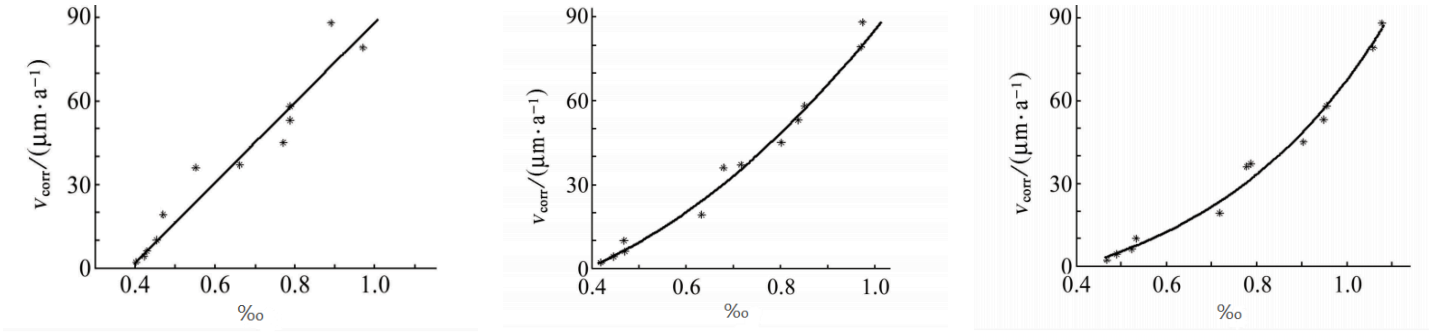

$v_{corr} = 132.1t - 51.6$

(a) linear regression model

$v_{corr} = 102.7t^2 - 16.4t - 10.9$

(b) quadratic function regression model

$v_{corr} = e^{(2.53t+1.97)} - 20.2$

(c) exponential function regression model

Fig. 15. Fitted model of sulfur corrosion in steel

where v_{corr} is the corrosion rate, and t is the thousandth of sulfur ions in any form (SO_4^{2-}, S^{2-}, SO_x).

As in the results, the corrosion models are fitted and not only S^{2-} ions are counted in the final calculation of research objects. For better understanding of the current project, an ideal numerical model is more efficient and universal in prediction of corrosion under the existence of various corrosive ions. Thus, further work is necessary to modify the models into summative ones by using the applicable test data. To achieve this, by referring the former research, experimental researches may be demanded in following study steps on sulfur ions.

2.3 Student Mentoring

During this quarter, three graduate students (Shuomang Shi, Ph. D. in Civil and Environmental Engineering at NDSU, Hafiz Usman Ahmed, Masters in Civil and Environmental Engineering at NDSU, and Jiapeng Lu, Ph.D. Student in chemistry at NDSU) and four undergraduate research assistants (Gina Blazanin, Alex Glowacki, Thomas Rasmussen, and Uuganbayar Ganselem) were hired to work on this project. The three graduate students will work on this project from Quarter 5 to Quarter 6 of this project. The four undergraduate students were hired from Jan 2020 to May 2020. New undergraduate research assistants will be hired in Sep 2020 for future quarters of this project.

2.4 Outreach Activities

In this quarter, we had our "CORE" outreach program again with CHARISM, a neighborhood-based program that works to provide opportunities to local youth and their families from low-income and refugee backgrounds to learn and connect. The workshop was planned to be eight lessons and we had six lessons to four different sites of after school programs. Unfortunately, due to COVID-19 and the widespread concern in our country and contamination, we were unable to finish out our final two lessons with CHARISM this spring after NDSU transitioned to remote learning and North Dakota public schools were suspended for the time being. The workshop was organized to be every Thursday afternoon from 3:30pm to 5:00pm starting from Feb 6th 2020. Three sites hosted elementary school students and one site hosted middle school students. In general, there are about 16 students in each site. Fig. 16 shows some photos of the activities performed in this outreach program. In total, there were more than 64 students

benefited from this outreach program. The feedback from the students indicated great interests generated in STEM area after attending this outreach program. In next quarter, we will try to conduct outreach to Native American students if the outbreak clears in summer and events are allowed.

Fig. 16. Activities in the CORE outreach program 2020

2.5 Future work

In the 7th quarter, there will be four objectives:

1) Task 2.1: Develop sensor film for the H^+/pH;
2) Task 2.2: Continue the simulation and experimental research on the survivability under oil/gas or water environment;
3) Task 2.2: Test and analyze more sensor film characteristics and continue quantify the color changes;
4) Task 3: Test parameters for corrosion model prediction.

References:

[1] Nor Roslina Rosli, "The Effect of Oxygen in Sweet Corrosion of Carbon Steel for Enhanced Oil Recovery Applications", Ph.D. Dissertation, Ohio University, Dec 2015.

[2] C. deWaard and D. E. Milliams, "Carbonic acid corrosion of steel," Corrosion, vol. 31, no. 5, pp. 177–181, 1975.

[3] L. G. S. Gray, B. G. Anderson, M. J. Danysh, and P. R. Tremaine, "Mechanism of Carbon Steel Corrosion in Brines Containing Dissolved Carbon Dioxide at pH 4," in CORROSION/1989, New Orleans, LA, 1989.

[4] S. Wang, K. George, S. Nesic, "High Pressure CO2 Electrochemistry and the Effect of Acetic Acid", CORROSION/2004, Paper No. 04375, (Houston, TX: NACE International, 2004).

[5] K. George, S. Nesic, K. de Waard, "Electrochemical Invesitgation of CO2 Corrosion of Mild Steel in the Presence of Acetic Acid", CORROSION, Paper No. 04379, 2004.

[6] Nordsveen, M., et al. "A mechanistic model for carbon dioxide corrosion of mild steel in the presence of protective iron carbonate films—part 1: theory and verification." Corrosion 59.5 (2003): 443-456.